Methane dissociation on the steps and terraces of Pt(211) resolved by quantum state and impact site

Helen Chadwick, Han Guo, Ana Gutiérrez-González, Jan Paul Menzel, Bret Jackson, and Rainer D. Beck

Citation: The Journal of Chemical Physics **148**, 014701 (2018);
View online: https://doi.org/10.1063/1.5008567
View Table of Contents: http://aip.scitation.org/toc/jcp/148/1
Published by the American Institute of Physics

Methane dissociation on the steps and terraces of Pt(211) resolved by quantum state and impact site

Helen Chadwick,[1,a)] Han Guo,[2] Ana Gutiérrez-González,[1] Jan Paul Menzel,[2,a)] Bret Jackson,[2,b)] and Rainer D. Beck[1,b)]
[1]*Laboratoire de Chimie Physique Moléculaire, Ecole Polytechnique Fédérale de Lausanne, 1015 Lausanne, Switzerland*
[2]*Department of Chemistry, University of Massachusetts, Amherst, Massachusetts 01003, USA*

(Received 7 October 2017; accepted 17 November 2017; published online 2 January 2018)

Methane dissociation on the step and terrace sites of a Pt(211) single crystal was studied by reflection absorption infrared spectroscopy (RAIRS) at a surface temperature of 120 K. The C—H stretch RAIRS signal of the chemisorbed methyl product species was used to distinguish between adsorption on step and terrace sites allowing methyl uptake to be monitored as a function of incident kinetic energy for both sites. Our results indicate a direct dissociation mechanism on both sites with higher reactivity on steps than on terraces consistent with a difference in an activation barrier height of at least 30 kJ/mol. State-specific preparation of incident CH_4 with one quantum of antisymmetric (ν_3) stretch vibration further increases the CH_4 reactivity enabling comparison between translational and vibrational activation on both steps and terraces. The reaction is modeled with first principles quantum theory that accurately describes dissociative chemisorption at different sites on the surface. *Published by AIP Publishing.* https://doi.org/10.1063/1.5008567

I. INTRODUCTION

The dissociation of small polyatomic molecules on transition metal surfaces often represents the rate limiting step in the heterogeneously catalyzed processes used to produce chemicals on an industrial scale.[1] Developing a predictive understanding of these dissociation reactions is not only of fundamental interest but also of practical importance.

In steam reforming, used commercially to produce hydrogen, the dissociation of methane on the transition metal catalyst is the rate determining step.[2] Experiments have shown that this reaction is non-statistical[3] with mode-specificity,[4–6] bond-selectivity,[5,7,8] and stereo-specificity[9,10] all being observed, making obtaining an accurate theoretical description challenging. Only very recently has quantitative agreement (within chemical accuracy, 4.2 kJ/mol) between experiment and theory been achieved by Kroes and co-workers using specific reaction parameter (SRP) density functional theory.[11,12] By using the initial reaction probability (S_0) for the dissociation of CHD_3 on Ni(111) from one experiment to optimize a single parameter in their calculations, they were able to reproduce S_0 obtained experimentally for CHD_3 dissociation both under laser-off conditions and prepared with a quantum of C—H stretch vibration on Ni(111), Pt(111) and Pt(211).

In previous quantum state-resolved studies of methane dissociation on transition metal surfaces,[13–17] only the total reactivity averaged over all impact sites on the surface has been determined. By combining quantum state-specific reactant preparation in a molecular beam with reflection absorption infrared spectroscopy (RAIRS) product detection, we demonstrate here that we can additionally resolve whether methane dissociates on the steps (red) or terraces (black) of a Pt(211) crystal (shown schematically in Fig. 1), allowing both quantum state-specific and site-resolved reactivity to be determined simultaneously. This additional level of resolution provides a further stringent test of theory, requiring that the reactivity determined from calculations can also be resolved by impact site on the surface. Here, we use 15-dimensional quantum reactive scattering methods based on the Reaction Path Hamiltonian (RPH) approach[18–24] to calculate site-resolved values of S_0 which we compare to the values obtained experimentally. While traditional quantum methodologies for gas-surface scattering have advanced significantly in recent years,[25] our RPH approach remains the only method that can accurately include and describe all of the vibrational modes of methane.

II. EXPERIMENTAL METHODS

The experimental apparatus has been described in detail previously,[26] and only the most relevant details will be presented here. In brief, the experiments were performed in a surface science machine consisting of a triply differentially pumped molecular beam source chamber attached to an ultrahigh vacuum (UHV) chamber with a base pressure of 5×10^{-11} mbar. The single crystal Pt(211) surface, cut to within 0.1° of the (211) plane, was mounted in the UHV chamber in a tantalum support between two tungsten wires. A K-type thermocouple was spot welded to the tantalum mount

[a)]Current address: Leiden Institute of Chemistry, Gorlaeus Laboratories, Leiden University, P.O. Box 9502, 2300 RA Leiden, The Netherlands.
[b)]Electronic addresses: jackson@chem.umass.edu and rainer.beck@epfl.ch

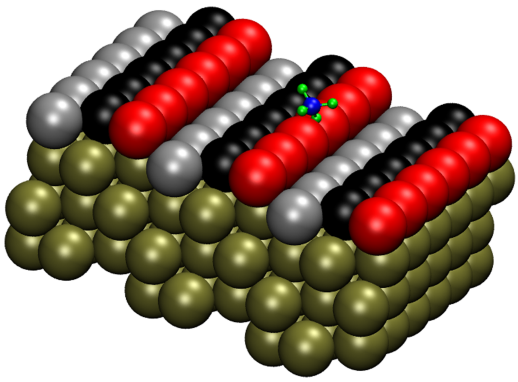

FIG. 1. The Pt(211) surface has three atom wide (111) terraces and one atom high (100) steps. We label the row of atoms on the step edge as step (red), the middle row terrace (black), and the final row corner (gray).

to monitor the temperature, which was stabilized to within 1 K. From temperature programmed desorption measurements, we estimate that there was a maximum of 10 K difference between the temperature of the tantalum mount and the Pt(211) surface. The surface could be heated to over 1100 K by passing a current along the tungsten wires and cooled to 100 K through the thermal contact with a liquid nitrogen reservoir. Between deposition measurements, the Pt(211) crystal was cleaned by exposure to 5×10^{-8} mbar of O_2 at 700 K before annealing at 1100 K. At the end of each day, cleaning by Ar^+ sputtering and annealing at 1100 K was used. The surface cleanliness was confirmed using Auger electron spectroscopy.

The molecular beam was formed by expanding 2 bars of a 3% CH_4 seeded in He gas mix through a stainless steel nozzle with a 50 μm diameter hole before passing through a 2 mm diameter skimmer. To change the incident kinetic energy (E_k) of the molecules, the nozzle was resistively heated to temperatures of up to 800 K. The nozzle temperature was monitored by a K-type thermocouple spot welded to the end of the nozzle and stabilized to within 1 K. The velocity distribution of the molecular beam was measured by the time of flight method using a fast chopper wheel in conjunction with an on-axis quadrupole mass spectrometer (QMS). The experimental distribution of CH_4 arrival times was fit by a flux weighted Maxwell Boltzmann distribution.[27] During the molecular beam deposition, CH_4 was incident perpendicular to the plane of the Pt(211) surface. The CH_4 flux incident on the Pt(211) surface was monitored using an off-axis QMS calibrated against a cold-cathode ion gauge.

For the laser-on measurements, a fraction of incident methane was prepared quantum state selectively in the antisymmetric C—H stretch fundamental vibration $\nu_3 = 1$, $J = 2$ *via* the R(1) transition using a continuous wave optical parametric oscillator. The laser frequency was stabilized to the ($\nu_3 = 1, J = 2 \leftarrow \nu = 0, J = 1$) transition frequency of 3038.490 cm^{-1} by locking to a Lamb-dip[10] created in a static absorption cell containing 30 μbar methane. We excite the molecular beam using rapid adiabatic passage[28] (RAP) by focusing the laser with a 254 mm focal length cylindrical lens to create curved wavefronts in the region where the molecular beam traverses the laser beam. CH_4 molecules passing through the focused laser beam experience a frequency sweep due to the Doppler effect which, providing certain conditions are met, can completely transfer the population of the initial rovibrational state to the final rovibrational state. A room temperature pyroelectric detector was used to determine the flux of state prepared molecules created by RAP.

We recorded the methyl uptake resulting from exposure of the Pt(211) surface to an incident molecular beam of CH_4 at a surface temperature (T_S) of 120 K, where the nascent methane dissociation products CH_3(ads) and H(ads) are stable. CH_3 adsorbed on Pt(211) was detected by the RAIRS technique using a Bruker Vertex V70 Fourier transform infrared spectrometer with an external liquid nitrogen cooled InSb detector. Each RAIRS spectrum was recorded with 4 cm^{-1} resolution averaging over either 256 scans or 512 scans, corresponding to an acquisition time of approximately 30 s or 1 min. To convert the spectra to uptake curves, we fit the spectra to the sum of two Gaussians to obtain the area of the absorption peaks for CH_3(ads) on the step and terrace. The full width at half maximum (FWHM) of both peaks were on the order of 5 cm^{-1}–8 cm^{-1}. As the RAIRS spectra were recorded with a resolution of 4 cm^{-1}, the FWHM of each peak showed significant scatter around the general trend, with the problem then transferred to the calculated area. To reduce the noise in the area of the spectra, the FWHM of the spectra were fit to a logarithm function, and the FWHM from this fit used with the peak height obtained from the Gaussian fit to obtain the absorption area which is presented as the CH_3 RAIRS absorption signal.

The flux of methane molecules impinging on the surface was calculated using[29]

$$\text{Flux} = \frac{\Delta PS}{Ak_B T_g}, \tag{1}$$

where ΔP is the methane partial pressure rise when the molecular beam enters the UHV chamber obtained from the calibrated off-axis QMS, S is the experimentally determined pumping speed of the UHV chamber for CH_4 (520 l/s), A is the area of the molecular beam spot on the surface determined by Auger electron spectroscopy, k_B is Boltzmann's constant, and T_g is the temperature of the static gas in the UHV chamber (298 K). The dose is the product of incident flux multiplied by the deposition time. For the laser-on measurements, we take into account the excited fraction (f_{exc}) of the incident CH_4($\nu_3 = 1$, $J = 2$) prepared by RAP.

III. THEORETICAL METHODS

Electronic structure calculations are performed using the Density Functional Theory (DFT)-based Vienna *ab initio* simulation package (VASP), developed at the Institut für Materialphysik of the Universität Wien.[30–34] A four-layer 3 × 2 supercell with periodic boundary conditions is used to represent the metal as a series of infinite slabs, with a large vacuum space of 16 Å between the slabs. The interactions between the ionic cores and the electrons are described by fully nonlocal optimized projected augmented-wave (PAW) potentials.[34,35] The exchange-correlation effects are treated within the generalized gradient approximation using the Perdew-Burke-Ernzerhof

(PBE) functional.[36,37] We also use the SRP functional developed by the Kroes group in Leiden,[11,12] which has been shown to accurately describe the dissociative chemisorption of methane on both Ni and Pt surfaces.[11,12,38] The SRP functional consists of a combination of PBE[36,37] and Revised PBE (RPBE)[39] for exchange and vdW-DFT[40] for correlation.

Our Hamiltonian for dissociation over a rigid metal lattice is

$$H = K + V = -\frac{\hbar^2}{2}\sum_{i=1}^{15}\frac{\partial^2}{\partial x_i^2} + V(x_1, x_2, ..., x_{15}), \qquad (2)$$

where x_i are the 15 mass-weighted Cartesian coordinates of the CH_4 nuclei. To construct our potential energy surface (PES), we first locate all relevant transition states (TSs) and the corresponding minimum energy paths (MEPs) for reaction. We do not relax the metal lattice in the presence of CH_4 because we model a high-energy collision where the lattice does not have time to relax during the collision. We have characterized four transition states for dissociative chemisorption: dissociation along the step edge (path N), dissociation across the edge (paths M and L), and dissociation over a terrace atom. Details are presented in Sec. IV. In Fig. 2, we plot the total energy, $V_0(s)$, along the L and N MEPs, as a function of the distance along the path, s, where $(ds)^2 = \sum_{i=1}^{15}(dx_i)^2$; $s = 0$ at the TS. For comparison, we also plot the MEP for dissociation on Pt(111), which is similar to that on the Pt(211) terrace, except for a change in the barrier height.

At several dozen images along each reaction path, we compute and diagonalize the force-projected Hessian to get the fourteen normal vibrational coordinates, Q_k, and corresponding frequencies, $\omega_k(s)$, describing harmonic motion orthogonal to the reaction path. Ignoring higher order (anharmonic) terms, our PES can be written in the reaction path coordinate s and $\{Q_k\}$,

$$V = V_0(s) + \sum_{k=1}^{14}\frac{1}{2}\omega_k^2(s)Q_k^2. \qquad (3)$$

We write our molecular wave function, in reaction path coordinates, as

$$\Psi(t) = \sum_{\mathbf{n}}\chi_{\mathbf{n}}(s;t)\,\Phi_{\mathbf{n}}(\{Q_k\};s), \qquad (4)$$

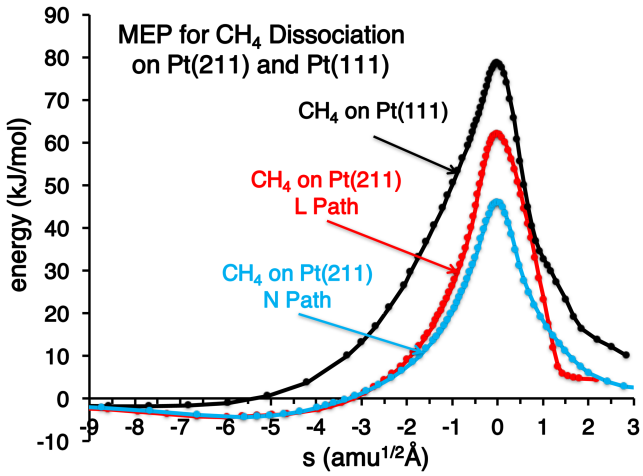

FIG. 2. Reaction paths for methane dissociation on Pt(211) and Pt(111).

where Φ_n are the products of harmonic oscillator eigenfunctions that depend parametrically on s, and the vector **n** labeling the vibrational states corresponds to a set of quantum numbers n_k. The equations of motion for the wave packets, $\chi_{\mathbf{n}}(s;t)$, are[20]

$$i\hbar\frac{\partial\chi_{\mathbf{n}}(s;t)}{\partial t} = \left[\frac{1}{2}p_s^2 + V_0(s) + \sum_{k=1}^{14}\hbar\omega_k(s)\left(n_k + \frac{1}{2}\right)\right]\chi_{\mathbf{n}}(s;t) + \sum_{\mathbf{n}'}F_{\mathbf{n}\mathbf{n}'}\chi_{\mathbf{n}'}(s;t). \qquad (5)$$

The wave packets evolve on vibrationally adiabatic potential energy surfaces for each vibrational state **n**, and the operators $F_{\mathbf{n}\mathbf{n}'}$ couple states of the same symmetry. $F_{\mathbf{n}\mathbf{n}'}$ are proportional to the vibrationally nonadiabatic couplings computed from the normal mode eigenvectors. Because of the parametric dependence of $\Phi_{\mathbf{n}}$ on s, $F_{\mathbf{n}\mathbf{n}'}$ also contain momentum operators, p_s, and curve crossing (transitions between vibrationally adiabatic states) becomes more probable at higher velocities as well as for larger values of the coupling. The sums over **n** in Eqs. (4) and (5) include the vibrationally adiabatic ground state and all states with either one or two vibrational quanta in the nine normal modes of the incident molecule. A detailed derivation can be found in a recent publication.[22] For a given initial vibrational state, $\mathbf{n_0}$, standard techniques are used to evolve the wave packets[19,20] and energy-analyze the reactive flux.[41,42] The result is the rigid-lattice reaction probability, $P_0(E_k, \mathbf{n_0})$, for collision at a surface impact site corresponding to one of the 4 MEPs. The rotational orientation of the molecule has been allowed to evolve adiabatically.

To compute S_0, we first average P_0 over all surface impact sites assuming sudden behavior for X and Y, the location of the molecular center of mass over the surface unit cell. Motion along X and Y should be slow on collisional time scales, given the normal incident conditions. *Ab initio* molecular dynamics (AIMD) studies confirm that there is little translational steering.[21] We divide the Pt(211) surface into three regions: the step region, the terrace region, and the corner region, as shown schematically in Fig. 1. We assume that the corner region contributes nothing to S_0, given the large barrier. We average P_0 for the terrace over all impact sites within that region, using the following to approximate P_0 at impact sites (X,Y) close to the minimum barrier site at X = 0, Y = 0:

$$P_0(E_i, \mathbf{n_0}; X, Y) \approx P_0(E_i - \Delta V, \mathbf{n_0}; 0, 0). \qquad (6)$$

$\Delta V(X,Y)$ is the increase in barrier height relative to the minimum barrier site. We can approximate this using the normal modes or compute it directly using DFT for several molecular configurations near the TS. We take a similar approach for the step, though that region is broken up into sub-regions corresponding to the M, N, and L reaction paths.

AIMD also suggests that the rotational behavior might be closer to sudden at high incident E_k.[21,43] To compute the sticking in the rotationally sudden limit, we use a similar approach to Eq. (6), averaging over orientations of the molecule at the TS, as described in a recent study.[24] As in that work, we then use a switching function to combine these two results so that final $S_0(E_k)$ is 90% rotationally adiabatic at E_k = 0.2 eV and 90% rotationally sudden at E_k = 0.9 eV.

We treat lattice motion using a sudden model described elsewhere.[44,45] Given the metal atom mass and the short collision times, we assume the lattice atom is stationary during the collision. On Ni and Pt surfaces, as the lattice atoms vibrate the height of the barrier to methane dissociation changes. On the (100) and (111) surfaces of Ni and Pt and for the Pt(211) terrace atoms, this is mostly confined to the motion, normal to the surface, of the metal atom over which the methane dissociates.[44,45] If Q is the displacement of this lattice atom in and out of the plane of the surface and Q > 0 for motion away from the bulk, the barrier height changes by an amount $-\beta Q$, where β = 91.9 kJ/(mol/Å) on Pt(111).[46] We average the sticking probability over all values of Q, using a Debye model for the probability of having a value of Q for a given T_S. To do this, we need to know the root mean square value for Q, Q_{rms}, at some T_S. We have typically gotten this from surface scattering experiments, but such data are not available for Pt(211) nor are such data site specific. We have thus used AIMD with our Pt(211) slab to compute Q_{rms} at 300 K. We find that for the terrace atom, Q_{rms} = 0.109 Å in the direction normal to the (111) terrace, very similar to the Q_{rms} value of 0.104 Å on Pt(111). On the step edge, the behavior is more complex. We find β = 119.7 and 96.3 kJ/(mol/Å) for the L and N paths, respectively, but Q has components both normal and lateral to the surface, away from the edge. The motion of other atoms can also modify the barrier, but their contributions are small. Our AIMD calculations give Q_{rms} = 0.099 Å for the motion of step atoms in the direction perpendicular to the surface at 300 K. For motion lateral to the surface, Q_{rms} is not significantly different from this. Lattice vibration also changes the location of the TS along Z. We find that as the lattice is displaced normal to the (211) surface by Q_Z, the location of the TS changes by αQ_Z, where α = 0.8379 and 0.8993 for the L and N paths, respectively. We use the modified surface mass model[47] to include this effect.

IV. RESULTS AND DISCUSSION

It is well known that CH_4 dissociates on Pt(111) by a direct reaction and that a single C—H bond is broken, leading to chemisorbed products CH_3(ads) and H(ads).[8,26,48–50] CH_3(ads) on Pt(111) adsorbs on top of a Pt atom and is stable at T_S below 200 K[49] and can be detected by RAIRS *via* absorption peaks at 2883 cm^{-1} and 2755 cm^{-1} [Fig. 3(a) top] assigned to the symmetric CH_3(ads) stretch[26,50,51] and the first overtone of the antisymmetric bend, respectively. For dissociation of CH_4 on Pt(211), we observe two peaks in the CH_3(ads) stretch region at 2886 cm^{-1} and 2903 cm^{-1} [Fig. 3(a) bottom] which we assign by comparison with the spectrum for Pt(111) to the symmetric stretch of CH_3(ads) on terrace and step sites, respectively. The assignment of the 2903 cm^{-1} peak to CH_3(ads) on step sites is supported by the observation of much higher reactivity for this site (see Fig. 3) consistent with the calculated dissociation barrier heights for step, terrace, and corner sites (Table II).

We attribute the additional peak at 2752 cm^{-1} to the bend overtone of the CH_3(ads) on both sites. The detection of two peaks in the C—H stretch region of the RAIRS spectrum rather than three suggests that the corner sites

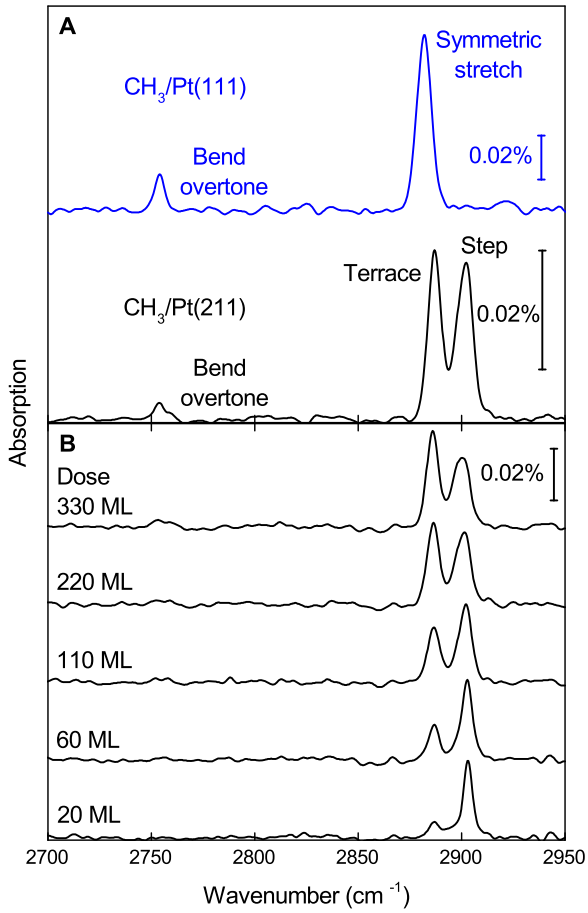

FIG. 3. (a) Comparison of the RAIRS spectra of CH_3(ads) on Pt(111) (top, blue) and Pt(211) (bottom, black) at T_S = 120 K. (b) Variation of the RAIRS spectra for CH_3(ads) with incident methane dose at T_S = 120 K and E_k = 65 kJ/mol.

are not occupied by CH_3(ads) under the conditions of our experiments.

These observations are consistent with our DFT calculations. CH_3 prefers to bind on the top sites of Pt(111) and Pt(100),[52,53] and we find similar behavior on Pt(211). The adsorption energies for the three Pt(211) top sites are listed in Table I. Adsorption at the step edge is the most stable. We find that adsorption of CH_3 on the top sites of Pt(111) is very similar to that on the Pt(211) terrace atoms. The most stable H adsorption is on the bridge site along the step edge, with an adsorption energy of 275 kJ/mol, 13 kJ/mol larger than the second most stable state. In Table II, we summarize the properties of the four most important transition states for the

TABLE I. The adsorption energy for CH_3 at step, terrace, and corner top sites on Pt(211) and the top site on Pt(111). E_{ads}^{PBE} and E_{ads}^{SRP} are adsorption energies with lattice atoms unrelaxed, using PBE and SRP functionals, respectively. $E_{ads}^{SRP,relax}$ is the adsorption energy when the top two layers of the metal lattice are allowed to relax.

	E_{ads}^{PBE} (kJ/mol)	E_{ads}^{SRP} (kJ/mol)	$E_{ads}^{SRP,relax}$ (kJ/mol)
Pt(211) step	−204	−210	−215
Pt(211) terrace	−178	−194	−209
Pt(211) corner	−112	−123	−159
Pt(111) top	−189	−194	−206

TABLE II. Transition state data for methane dissociation on Pt(211) and Pt(111). $Z_C^{\ddagger}$ is the distance from the C atom to the Pt atom directly below it. $r^{\ddagger}$ and $\theta^{\ddagger}$ are the length of the dissociating bond and its angle relative to the surface normal, respectively. E_b is the barrier height relative to the methane infinitely far from the surface, and E_a, the activation energy, is E_b with zero point energy (ZPE) corrections. All results are in kJ/mol and are for the PBE functional, except for E_a^{SRP}, the activation energy using the SRP functional.

	$Z_C^{\ddagger}$ (Å)	$r^{\ddagger}$ (Å)	$\theta^{\ddagger}$ (Å)	E_b	*ZPE*	E_a	E_a^{SRP}
Pt(211), N	2.242	1.480	133.6	46	−10	36	42
Pt(211), M	2.157	1.608	122.0	54	−7	47	47
Pt(211), L	2.175	1.654	124.3	62	−9	53	55
Pt(211), terr	2.254	1.525	129.4	101	−11	90	84
Pt(111)	2.241	1.521	131.7	79	−11	68	68

dissociation of CH_4 on Pt(211). Consistent with the strong product binding on the step edge, the lowest barrier is along path N, where the activation energy is only 42 kJ/mol. For all transition states, the carbon atom is approximately above the top site with the reactive C—H bond angled toward the metal. The N transition state geometry, with the carbon over an edge atom and the breaking C—H bond oriented parallel to the edge, is consistent with that reported in other studies on Pt(211).[12] For the M and L transition states, the carbon is also over an edge atom, but the dissociating bond is oriented perpendicular to the step edge, with the reactive H toward the (111) terrace for the M path and toward the (100) step for the L path. This geometry allows the carbon to get closer to the Pt at the TS, and the bond is stretched a bit more. The calculated activation energy for dissociation over a Pt(211) terrace atom is 84 kJ/mol, larger than that on Pt(111) (68 kJ/mol) or any of the edge sites. The terrace TS structure is very similar to that on Pt(111), taking into account that the (111) terrace of Pt(211) is not perpendicular to the surface normal. For the Pt(211) corner atoms, the CH_3(ads) binding energy is only 123 kJ/mol, and we estimate that the barrier for dissociation is 183 kJ/mol. Thus, dissociation is not likely to occur at the corner sites at the molecular energies considered in this study.

We find that our peak assignment for CH_3(ads) is reversed compared to those previously reported for CO on the steps and terraces of Pt(211)[54,55] and on curved Pt crystals.[56] For CO(ads) on steps, the C═O stretch is lower in frequency than for adsorption on the terrace site, whereas for CH_3(ads) the step peak is 17 cm^{-1} higher in frequency than the terrace peak. The redshift for the CO stretch on the steps is rationalized by weakening of the C═O bond due to electron transfer from the metal to $2\pi^*$ orbitals of CO leading to a stronger bond softening for CO on the step edges. For the CH_3(ads), our RAIRS data indicate the opposite trend: stronger C—H bond softening occurs on the terrace site consistent with calculations reported by Michaelides and Hu.[57] These authors examined the C—H stretch frequency of CH_3(ads) on top and threefold hollow sites on Pt(111) and Ni(111) and calculated a stronger redshift for the hollow sites due to the C—H bonds being closer to the metal atoms than for the top sites, consistent with experimental values for CH_3(ads) on Ni(111) and Pt(111). We do not observe the same splitting in the overtone of the bend, showing this vibration is affected less by this bond softening.

The non-invasive nature of RAIRS allows us to monitor the simultaneous, site-selective uptake of CH_3(ads) on step and terrace sites by recording spectra throughout a CH_4 deposition experiment. Figure 3(b) presents RAIRS spectra taken during a measurement at E_k = 65 kJ/mol, T_S = 120 K without laser excitation. The higher frequency peak appears first, consistent with CH_4 dissociation on the more reactive steps. As the step peak saturates, the peak at 2886 cm^{-1} grows more slowly in intensity indicating CH_3(ads) on the terraces. With increasing CH_3(ads) coverage on the terraces, the higher frequency step peak broadens, most likely due to interaction between CH_3(ads) on steps and on terraces.

Employing the analysis described in Sec. II, the RAIRS spectra are converted into the uptake curves shown in Fig. 4, where the CH_3 RAIRS signal is plotted as a function of the incident methane dose for uptake on the steps (red points) and terraces (black points) for measurements without laser excitation (left-hand column) and laser-on depositions where between 10% and 45% of the incident methane is prepared with a single quantum of antisymmetric stretch (ν_3) vibration (right-hand column). At E_k = 40 kJ/mol without laser excitation, uptake is only observed on the steps. Increasing E_k or adding a quantum of ν_3 vibration leads to CH_3(ads) uptake on both steps

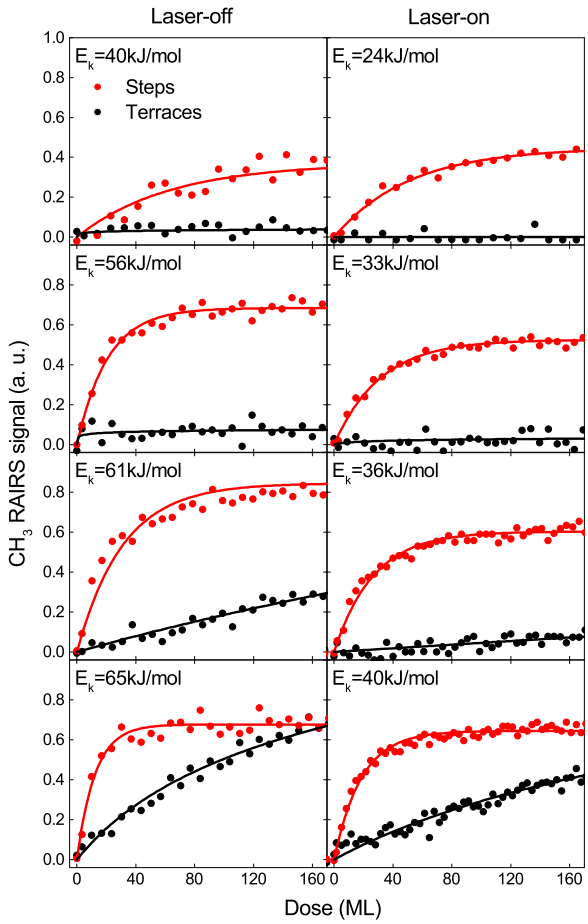

FIG. 4. Uptake curves measured under laser-off (left panels) and laser-on (right panels) conditions for dissociation of methane on the steps (red points) and terraces (black points) on Pt(211) at T_S = 120 K. The solid lines are fits to the data obtained using Eq. (7).

and on the terraces, demonstrating that methane dissociation on Pt(211) is promoted by both translational and vibrational energy.

Without laser excitation, CH_3(ads) uptake is first seen on the steps of Pt(211) at E_k = 33 kJ/mol (data not shown) and on the terraces at E_k = 61 kJ/mol. From these values, we estimate the activation barrier on the step to be at least 30 kJ/mol lower than the activation barrier on the terrace. This is consistent with calculated values of 42 and 37 kJ/mol for the difference between the activation energy on the terrace and on the two lowest barrier sites on the step edge. The experimental value establishes only a lower limit for the true difference in activation barriers as the increase in E_k was achieved by nozzle heating, which will thermally populate low lying bending vibrations of CH_4. With increasing nozzle temperature, more molecules are in vibrationally excited states, leading to a stronger increase in reactivity than would be expected from increasing only E_k.

The theoretical activation barriers were calculated for methane dissociation on a clean Pt(211) surface, whereas the RAIRS uptake curves above show that there is significant CH_3(ads) on the steps when methane dissociation is observed on the terraces. As E_k increases, the maximum (saturation) CH_3(ads) coverage on the Pt(211) surface increases, as shown by the increasing asymptotes of the uptake curves for both the laser-off and laser-on data. The saturation coverage of CH_3(ads) on the steps also decreases slightly when there is significant CH_3(ads) uptake on the terrace. Both these observations suggest that CH_3(ads) increases the effective activation barrier height for methane dissociation compared to that on a clean Pt(211) surface, as has been observed previously on Pt(111).[58] DFT calculations in that work showed that this was due to substantial charge transfer between the metal and the adsorbed molecules, leading to repulsive forces between the dissociating CH_4 and CH_3(ads).[58]

A previous study on the dissociative chemisorption of methane on the stepped Pt(322) and Pt(355) surfaces performed at $T_S \approx 120$ K suggested that CH_3(ads) formed on the terraces migrated to the steps.[59] The uptake curves presented in Fig. 4 show no evidence of CH_3(ads) migration from step to terrace sites on Pt(211) at T_S = 120 K. If the methane dissociated on the terraces and the resultant CH_3(ads) migrated to the steps, then uptake on the terraces should only be detected once the steps are saturated, which is inconsistent with the data shown in Fig. 4. Furthermore, we detect no change in the RAIRS signal for the steps and terraces due to CH_3(ads) migration from the terraces to steps when the CH_4 deposition is stopped before the steps are saturated. These observations are fully consistent with our DFT calculations. Using the SRP functional and allowing the top two layers of the metal to fully relax, the computed activation energy for CH_3(ads) diffusion from the terrace to the more stable step site is 64.4 kJ/mol, and the corresponding rate constant is only about 10^{-15} s^{-1} at 120 K.

The reactivity of the methane on the step and terrace sites can be quantified by the initial sticking coefficient which is the probability that the molecule dissociates on either the step [S_0(step)] or the terrace [S_0(terr)] on the clean Pt(211) surface. This value is proportional to the initial gradient of the uptake curves presented in Fig. 4. Increasing E_k or adding a quantum of ν_3 leads to an increase in both S_0(step) and S_0(terr) as more incident energy is available to overcome the activation barrier for the dissociation. To be able to obtain absolute values of S_0, the data were fit using a Langmuir type uptake model,

$$\frac{d\Theta}{d\varepsilon} = S_0\,(1 - n_s\Theta)\,, \tag{7}$$

where Θ is the coverage, ε is the dose, and n_s is the number of sites that each adsorbate blocks on the surface. Each uptake was fit independently, i.e., assuming that the uptake of CH_3(ads) on the terrace was not influenced by CH_3(ads) uptake on the steps and vice versa.

In order to be able to fit the data, it is necessary to convert the CH_3 RAIRS signal to CH_3(ads) coverage. King and Wells (K&W) measurements[60,61] were used to determine the conversion for the step sites. Deposition measurements were done at E_k = 65 kJ/mol and were monitored using K&W and RAIRS (64 scans/spectra) simultaneously. We assumed that under these conditions, S_0(terr) made a negligible contribution to the sticking coefficient obtained from the K&W measurement. The RAIRS data were analyzed as above to obtain the uptake curve of the CH_3 RAIRS signal against the dose. The y axis was then scaled so that the initial gradient of the uptake curve matched the value of S_0 obtained from the K&W measurement. This procedure was repeated five times, and the average result was used as the conversion from the CH_3 RAIRS signal to coverage for all the uptake curves on the steps. The conversion factor for the terraces was taken to be the same as that for CH_3(ads) on a Pt(111) surface.

The state-resolved sticking coefficients, $S_0^{\nu_3}$, were found from the laser-off (S_0(laser-off)) and laser-on (S_0(laser-on)) sticking coefficients using[14]

$$S_0^{\nu_3} = \frac{S_0(\text{laser-on}) - S_0(\text{laser-off})}{f_{\text{exc}}} + S_0(\text{laser-off}). \tag{8}$$

In Fig. 5, the values of S_0(step) [filled points, panel (a)] and S_0(terr) [filled points, panel (b)] are compared with those calculated using the RPH model (solid lines and open points) described in Sec. III.[19–24] Good agreement between theory and experiment is observed for dissociation on the step sites, where the experimental S_0(step) has been calibrated using K&W measurements.[60,61] Theory also confirms that contributions to the total sticking from reactions on the terrace sites is negligible at E_k = 65 kJ/mol, as was assumed in the calibration of S_0(step). The theoretical laser-off values were estimated by including contributions from vibrationally excited states at the experimental nozzle temperatures. Given the low activation barriers and large S_0 for the ground state reaction at the step edge, these effects are relatively minor in Fig. 5(a). Finally, we note that S_0 computed using the PBE functional gives a reasonable agreement with experiment (not shown). However, rescaling our MEP barrier heights to the SRP values leads to the improved agreement in Fig. 5(a).

The agreement between theory and experiment for dissociative sticking on the terrace sites is less good. However, experimental S_0(terr) were estimated using the same conversion factor obtained for Pt(111).[26] It is clear from

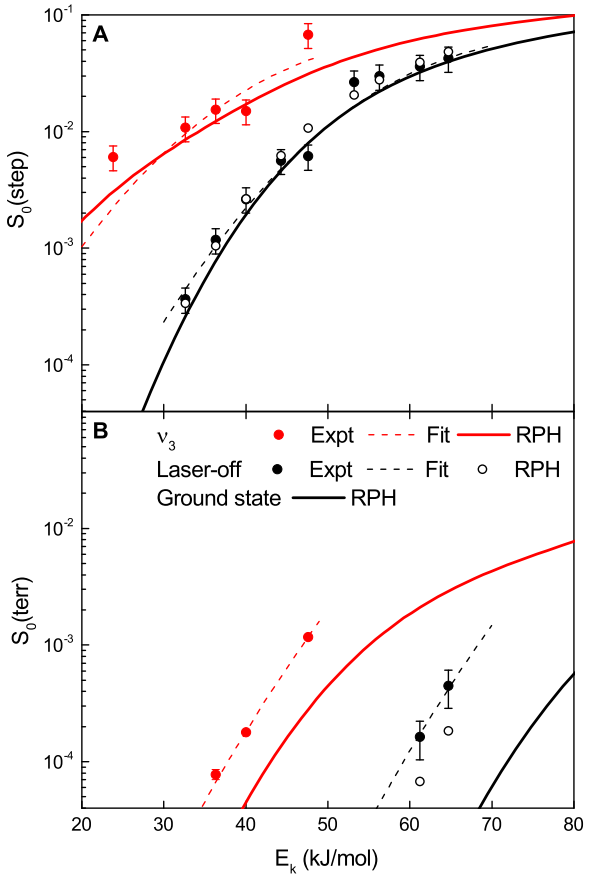

FIG. 5. (a) A comparison of experimentally determined state-resolved sticking coefficients for CH_4 prepared with a single quantum of ν_3 (red symbols) and under laser-off conditions (black symbols) for dissociation on the steps of Pt(211) at T_S = 120 K with those obtained from RPH calculations using the SRP functional (solid lines). The dashed lines are S-shape curve fits to the experimental data using Eq. (9). (b) As panel (a) but for dissociation on the terraces.

Table II that the energetics of methane chemisorption on the terraces of Pt(111) and Pt(211) are different, and the magnitude of the derivative dipole coupling for the symmetric stretch is likely to be different for CH_3 adsorbed on these two sites. If we rescale the experimental S_0(terr) by 0.3, the agreement improves significantly. Note that for the higher activation barriers and smaller values of sticking at the terrace sites, the laser-off corrections are much more important.

It is interesting to compare the contributions to the total sticking from the 4 primary reaction pathways. In Fig. 6, we plot the computed contributions to the total dissociative sticking probability from the four reaction paths, at T_S = 120 K, for the PBE functional. For molecules initially in the ground state, the contribution to the reactive sticking from the N MEP is an order of magnitude larger than that from any other path, except at the highest energies, where other paths can contribute several percent. Excitation of the antisymmetric stretch ($1\nu_3$) promotes reaction at all sites. The vibrational enhancement is largest for the L and M paths and for dissociation on the terrace sites. This is consistent with the elongation of the reactive bond at the transition state being larger for these paths (see Table II).

To compare the effect of adding kinetic or vibrational energy, the experimental data were fit using S-shape curves

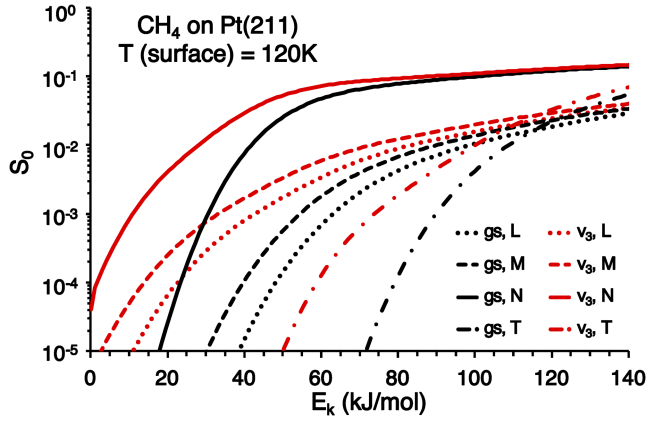

FIG. 6. Computed contributions to the dissociative sticking probability of methane from the three step (L, M, N) and one terrace (T) transition states. Results are shown for methane initially in the ground state (gs) and the $1\nu_3$ excited state, at T_S = 120 K.

(dashed lines, Fig. 5) given by[14,62]

$$S_0(E_k) = \frac{A}{2}\left[1 + \mathrm{erf}\left(\frac{E_k - E_0}{W}\right)\right], \tag{9}$$

where A is the asymptotic value of S_0 at infinitely high incident energy, E_0 is the average activation barrier height, and W is the width of the distribution of activation barriers. The laser-off and ν_3 data were fit simultaneously with A and W restricted to be the same for both sets of data. In the fit, each value of S_0 was weighted by $1/\sigma$, where σ is the error bar on the experimental data representing 68% confidence limits. The vibrational efficacy (η^{ν_3}) for each site on the surface was then found using[62]

$$\eta^{\nu_3} = \frac{(E_0(\text{laser-off}) - E_0(\nu_3))}{E_{vib}}, \tag{10}$$

where E_{vib} is the vibrational energy of a single quantum of antisymmetric stretch vibration (36 kJ/mol). The efficacy quantifies the relative efficiency with which vibrational energy promotes reactivity compared to the same amount of kinetic energy. η^{ν_3}(step) = 0.45 and η^{ν_3}(terr) = 0.59, showing adding a quantum of ν_3 promotes the reactivity more on the terraces of Pt(211) than the steps but that kinetic energy is more efficient on both sites. The efficacies extracted from the theoretical sticking curves typically vary with S_0. We find that the computed step efficacies vary over the range of the data from η^{ν_3}(step) = 0.50 at $S_0 = 3 \times 10^{-3}$ to η^{ν_3}(step) = 0.37 at $S_0 = 10^{-1}$, in good agreement with experiment. On the other hand, for the terrace site, we find that η^{ν_3}(terr) = 0.79 at $S_0 = 10^{-4}$ and η^{ν_3}(terr) = 0.76 at $S_0 = 10^{-3}$. However, we note that the experimental efficacies are computed relative to the laser-off curves, while the theoretical efficacies are relative to the true ground state. While this does not matter for reaction on the steps, we have shown that vibrationally excited molecules make a significant contribution to S_0(terr). If we compute the ν_3 efficacies relative to the two (theory) laser-off data points in Fig. 5(b), we find η^{ν_3}(terr) = 0.53 and 0.55, much closer to the experimental result. All of the above results are consistent with the reactive C—H bond being more stretched at the transition state for dissociation on the terrace site, 1.525 Å, than at the transition state for the dominant reaction path along the

step edge, 1.480 Å (see Table II). As discussed in several recent papers,[19–21,23,24,63,64] this vibrational enhancement in S_0 arises from a coupling of one of the antisymmetric stretch modes to the symmetric stretch, which correlates adiabatically with the dissociating bond. The sudden vector projection model proposed by Guo and co-workers provides another qualitative way to compare efficacies,[65] but we have not done such calculations here.

V. SUMMARY

It has long been proposed that reactions on most catalysts occur preferentially on step edges and other defect sites. We report here the results of a collaboration between experiment and theory that examines the dissociative chemisorption of methane on the stepped Pt(211) surface, where both the experimental and theoretical methods are resolved with respect to the reaction site and the quantum state of the incident molecule. The dissociative sticking of CH_4 produces H(ads) and CH_3(ads) fragments, and the methyl product is stable at our experimental surface temperature of 120 K. We demonstrate that it is possible to use RAIRS detection of the methyl fragment to distinguish between CH_3(ads) on the step and terrace atoms of Pt(211). The dissociative sticking of CH_4 is measured over a range of incident energies by using this site-specific RAIRS detection to monitor the formation of CH_3(ads) on the step and terrace sites. We find that the dissociation on Pt(211) is a direct reaction on both sites and that diffusion of the CH_3(ads) product does not occur at T_S = 120 K. CH_4 reactivity on Pt(211) is dominated by dissociation on step sites due to a lower barrier of at least 30 kJ/mol compared to the terrace sites. There is no evidence for dissociation at the corner sites on Pt(211).

DFT studies are consistent with these observations. Methyl groups prefer the top sites on Pt(211), and the binding is strongest over the atoms along the step. Consequently, the barriers are lowest there. We find that the activation energy for dissociation on the terrace is 84 kJ/mol, while on the step edge we find three transition states with activation energies of 42, 47, and 55 kJ/mol. The barrier for dissociation over the corner atoms is very large, 183 kJ/mol, and the reaction is not likely to occur there at the energies considered in this study. We also find that the barrier to methyl diffusion on the surface is large, 64 kJ/mol, and that diffusion should not occur at 120 K.

In the experimental sticking results, methane dissociation on both sites is promoted by adding kinetic energy or a single quantum of antisymmetric stretch vibration. First principles quantum scattering calculations of the dissociative sticking probability are in very good agreement with experiment for reaction at the step sites. For reaction at the terrace sites, the agreement is not as good, with experiment and theory differing by a factor of three. Unlike sticking on the step sites, it was not possible to independently calibrate sticking on the terrace. A factor of 3 is reasonable given variation in the RAIRS conversion factor and errors in the theory. Theory finds that reaction at the lowest barrier step site, where the molecule dissociates along the edge, dominates the sticking at all but the highest energies. The measured vibrational efficacy is found to be less than one on both the step and the terrace but is larger for dissociation on the terrace than on the step. This is consistent with our DFT studies, which find that the elongation of the dissociating bond is larger at the transition state for dissociation on the terrace than over the lowest barrier step site. Our calculations of sticking reproduce the experimentally measured efficacies for both the step and terrace sites.

ACKNOWLEDGMENTS

R.D.B., H.C., and A.G.-G acknowledge the financial support provided by the Swiss National Science Foundation (Grant Nos. P300P2-171247 and 159689/1) and the Ecole Polytechnique Fédérale de Lausanne.

[1] C. Stegelmann, A. Andreasen, and C. T. Campbell, J. Am. Chem. Soc. **131**, 8077 (2009).
[2] I. Chorkendorff and J. W. Niemantsverdriet, *Concepts of Modern Catalysis and Kinetics* (Wiley-VCH, Weinheim, 2003).
[3] R. R. Smith, D. R. Killelea, D. F. DelSesto, and A. L. Utz, Science **304**, 992 (2004).
[4] R. D. Beck, P. Maroni, D. C. Papageorgopoulos, T. T. Dang, M. P. Schmid, and T. R. Rizzo, Science **302**, 98 (2003).
[5] P. M. Hundt, H. Ueta, M. E. van Reijzen, B. Jiang, H. Guo, and R. D. Beck, J. Phys. Chem. A **119**, 12442 (2015).
[6] P. M. Hundt, M. E. van Reijzen, H. Ueta, and R. D. Beck, J. Phys. Chem. Lett. **5**, 1963 (2014).
[7] D. R. Killelea, V. L. Campbell, N. S. Shuman, and A. L. Utz, Science **319**, 790 (2008).
[8] L. Chen, H. Ueta, R. Bisson, and R. D. Beck, Faraday Discuss. **157**, 285 (2012).
[9] B. L. Yoder, R. Bisson, and R. D. Beck, Science **329**, 553 (2010).
[10] B. L. Yoder, R. Bisson, P. M. Hundt, and R. D. Beck, J. Chem. Phys. **135**, 224703 (2011).
[11] F. Nattino, D. Migliorini, G.-J. Kroes, E. Dombrowski, E. A. High, D. R. Killelea, and A. L. Utz, J. Phys. Chem. Lett. **7**, 2402 (2016).
[12] D. Migliorini, H. Chadwick, F. Nattino, A. Gutiérrez-González, E. Dombrowski, E. A. High, H. Guo, A. L. Utz, B. Jackson, R. D. Beck, and G.-J. Kroes, J. Phys. Chem. Lett. **8**, 4177 (2017).
[13] A. L. Utz, Curr. Opin. Solid State Mater. Sci. **13**, 4 (2009).
[14] L. B. F. Juurlink, D. R. Killelea, and A. L. Utz, Prog. Surf. Sci. **84**, 69 (2009).
[15] R. D. Beck and A. L. Utz, in *Dynamics of Gas-Surface Interactions: Atomic-Level Understanding of Scattering Processes at Surfaces*, edited by R. Dâiez Muiäno and H. F. Busnengo (Springer, Berlin, 2013).
[16] H. Chadwick and R. D. Beck, Chem. Soc. Rev. **45**, 3576 (2016).
[17] H. Chadwick and R. D. Beck, Annu. Rev. Phys. Chem. **68**, 39 (2017).
[18] W. H. Miller, N. C. Handy, and J. E. Adams, J. Chem. Phys. **72**, 99 (1980).
[19] B. Jackson and S. Nave, J. Chem. Phys. **138**, 174705 (2013).
[20] B. Jackson and S. Nave, J. Chem. Phys. **135**, 114701 (2011).
[21] B. Jackson, F. Nattino, and G.-J. Kroes, J. Chem. Phys. **141**, 054102 (2014).
[22] A. Farjamnia and B. Jackson, J. Chem. Phys. **142**, 234705 (2015).
[23] H. Guo and B. Jackson, J. Phys. Chem. C **119**, 14769 (2015).
[24] H. Guo and B. Jackson, J. Chem. Phys. **144**, 184709 (2016).
[25] B. Jiang, M. Yang, D. Xie, and H. Guo, Chem. Soc. Rev. **45**, 3621 (2016).
[26] L. Chen, H. Ueta, R. Bisson, and R. D. Beck, Rev. Sci. Instrum. **84**, 053902 (2013).
[27] G. Scoles, *Atomic and Molecular Beam Methods* (Oxford University Press, New York, 1988).
[28] H. Chadwick, P. M. Hundt, M. E. van Reijzen, B. L. Yoder, and R. D. Beck, J. Chem. Phys. **140**, 034321 (2014).
[29] M. R. Tate, D. Gosalvez-Blanco, D. P. Pullman, A. A. Tsekouras, Y. L. Li, J. J. Yang, K. B. Laughlin, S. C. Eckman, M. F. Bertino, and S. T. Ceyer, J. Chem. Phys. **111**, 3679 (1999).
[30] G. Kresse and J. Hafner, Phys. Rev. B **47**, 558 (1993).
[31] G. Kresse and J. Furthmüller, Comput. Mater. Sci. **6**, 15 (1996).
[32] G. Kresse and J. Furthmüller, Phys. Rev. B **54**, 11169 (1996).
[33] G. Kresse and J. Hafner, Phys. Rev. B **49**, 14251 (1994).
[34] G. Kresse and D. Joubert, Phys. Rev. B **59**, 1758 (1999).
[35] P. E. Blöchl, Phys. Rev. B **50**, 17953 (1994).
[36] J. P. Perdew, K. Burke, and M. Ernzerhof, Phys. Rev. Lett. **77**, 3865 (1996).
[37] J. P. Perdew, K. Burke, and M. Ernzerhof, Phys. Rev. Lett. **78**, 1396 (1997).

[38]F. Nattino, D. Migliorini, M. Bonfanti, and G.-J. Kroes, J. Chem. Phys. **144**, 044702 (2016).
[39]B. Hammer, L. B. Hansen, and J. K. Nørskov, Phys. Rev. B **59**, 7413 (1999).
[40]M. Dion, H. Rydberg, E. Schröder, D. C. Langreth, and B. I. Lundqvist, Phys. Rev. Lett. **92**, 246401 (2004).
[41]D. H. Zhang, Q. Wu, and J. Z. H. Zhang, J. Chem. Phys. **102**, 124 (1995).
[42]J. Dai and J. Z. H. Zhang, J. Phys. Chem. **100**, 6898 (1996).
[43]F. Nattino, H. Ueta, H. Chadwick, M. E. Van Reijzen, R. D. Beck, B. Jackson, M. C. Van Hemert, and G. Kroes, J. Phys. Chem. Lett. **5**, 1294 (2014).
[44]A. K. Tiwari, S. Nave, and B. Jackson, Phys. Rev. Lett. **103**, 253201 (2009).
[45]A. K. Tiwari, S. Nave, and B. Jackson, J. Chem. Phys. **132**, 134702 (2010).
[46]H. Guo, A. Farjamnia, and B. Jackson, J. Phys. Chem. Lett. **7**, 4576 (2016).
[47]A. C. Luntz and J. Harris, Surf. Sci. **258**, 397 (1991).
[48]J. Fan and M. Trenary, Langmuir **10**, 3649 (1994).
[49]D. H. Fairbrother, X. D. Peng, M. Trenary, and P. C. Stair, J. Chem. Soc., Faraday Trans. **91**, 3619 (1995).
[50]D. J. Oakes, M. R. S. McCoustra, and M. A. Chesters, Faraday Discuss. **96**, 325 (1993).
[51]I. J. Malik, M. E. Brubaker, S. B. Mohsin, and M. Trenary, J. Chem. Phys. **87**, 5554 (1987).
[52]S. Nave, A. K. Tiwari, and B. Jackson, J. Chem. Phys. **132**, 054705 (2010).
[53]S. Nave and B. Jackson, J. Chem. Phys. **130**, 054701 (2009).
[54]R. J. Mukerji, A. S. Bolina, and W. A. Brown, Surf. Sci. **527**, 198 (2003).
[55]S. C. Creighan, R. J. Mukerji, A. S. Bolina, D. W. Lewis, and W. A. Brown, Catal. Lett. **88**, 39 (2003).
[56]A. J. Walsh, R. van Lent, S. V Auras, M. A. Gleeson, O. T. Berg, and L. B. F. Juurlink, J. Vac. Sci. Technol. A **35**, 03E102 (2017).
[57]A. Michaelides and P. Hu, J. Chem. Phys. **114**, 2523 (2001).
[58]H. Ueta, L. Chen, R. D. Beck, I. Colón-Dìaz, and B. Jackson, Phys. Chem. Chem. Phys. **15**, 20526 (2013).
[59]C. Papp, B. Tränkenschuh, R. Streber, T. Fuhrmann, R. Denecke, and H.-P. Steinrück, J. Phys. Chem. C **111**, 2177 (2007).
[60]D. A. King and M. G. Wells, Surf. Sci. **29**, 454 (1972).
[61]H. Chadwick, A. Gutiérrez-González, and R. D. Beck, J. Chem. Phys. **145**, 174707 (2016).
[62]A. C. Luntz, J. Chem. Phys. **113**, 6901 (2000).
[63]K. G. Prasanna, R. A. Olsen, A. Valdés, and G.-J. Kroes, Phys. Chem. Chem. Phys. **12**, 7654 (2010).
[64]S. Nave, A. K. Tawari, and B. Jackson, J. Phys. Chem. A **118**, 9615 (2014).
[65]H. Guo and B. Jiang, Acc. Chem. Res. **47**, 3679 (2014).